This is a repository copy of *Modelled glacier response to centennial temperature and precipitation trends on the Antarctic Peninsula*.

White Rose Research Online URL for this paper:
http://eprints.whiterose.ac.uk/80649/

Version: Supplemental Material

Modelled glacier response to centennial temperature and precipitation trends on the Antarctic Peninsula

Bethan J. Davies, Nicholas R. Golledge, Neil F. Glasser, Jonathan L. Carrivick, Stefan R.M. Ligtenberg, Nicholas E. Barrand, Michiel R. van den Broeke, Michael J. Hambrey, John L. Smellie

Supplementary Information

1. Glaciological and geological input data

1.1 Glaciological and topographic data

Glaciological and topographical input data used to initialise the numerical model are derived from a number of sources. Glacier IJR45 (also known as 'Whisky Glacier'[1]) is one of the most intensely studied and instrumented glaciers on the northern Antarctic Peninsula, with an automatic weather station and surface mass balance measurements taken from 2009. Surface topography (5 m resolution digital elevation model, derived from aerial photographs taken in 2006), bed topography and ice-thickness data are available from the Czech Geological Survey and published data[1, 2]. Glacier IJR45 has an altitudinal range of 215-530 m a.s.l., and covers 2.4 km^2 excluding the debris-covered area. The bed slopes at ~5°, with bedrock in the upper reaches and subglacial till in the lower portion of the glacier[1]. The mean ice thickness is 99.6 ± 1.8 m and the maximum thickness is 158 ± 2 m. The glacier's velocity is 7.15 m a^{-1}, based on two years' measurements (pers. comm. from Z. Engel, March 2013, and our own unpublished field measurements). Glacier IJR45 currently has a net positive mass balance[3, 4], with high accumulation and ablation rates in the spring and summer (October-February), and negligible changes observed in winter[1]. The mean elevation is 340.6 ± 0.8 m a.s.l., the equilibrium line altitude is at 271 m a.s.l.[5], and the mean annual air temperature at 356 m a.s.l. is -7.8°C[1].

The longer-term (last 150 years) glacier behaviour is unknown and unconstrained. Satellite image analysis of the glacier's length and area detected no observable change from 1988-2009[5]. However, analysis of two digital elevation models derived from aerial photographs taken in 1979 and 2006 revealed a volume loss in the non-debris-covered area of 10.6%[1]. The area of bare ice shrank from 2.69 ± 0.02 km^2 to 2.40 ± 0.01 km^2. This equates to an annual rate of recession of 0.011±0.001 km^2 a^{-1} from 1979-2006. Surface elevations of the bare-ice area decreased by an average of 10.1±2.8 m over the period 1979-2006 (an annual rate of 0.37 ± 0.11 m a^{-1}). The greatest surface lowering occurred in the upper accumulation area of the glacier[1]. From 1979-2006, the volume of Glacier IJR45 reduced from 0.27 ± 0.02 km^3 to 0.24 ± 0.01 km^3, with a mean annual change of 0.001 ± 0.001 km^3 a^{-1}.

1.2 Prince Gustav Ice Shelf

Prince Gustav Ice Shelf was an unusual ice shelf with tributary glaciers from both Trinity Peninsula and James Ross Island, with flow units meeting in the centre of Prince Gustav Channel. These suture zones formed a zone of weakness along which extensive rifting occurred[6], prior to collapse in 1995 AD[7]. It was one of the first ice shelves around the Antarctic Peninsula to collapse[8]. High surface melt prior to collapse is

indicated by the extensive meltwater ponds observed on satellite imagery[6]. Following ice-shelf collapse, the tributary glaciers accelerated and thinned[6], and high rates of recession continue to present[5].

Marine geological data also indicate that Prince Gustav Ice Shelf was absent from 2-5 cal. ka BP[9, 10], when the James Ross Island ice core records temperatures around 0.5°C warmer than the 1961-1991 mean[11]. This suggests strong surface melting[12, 13], because ice-shelf removal normally occurs during periods of strong surface melt and meltwater ponding[13].

1.3 Glacial Geology on James Ross Island

Ulu Peninsula was inundated by the Antarctic Peninsula Ice Sheet during the Last Glacial Maximum[14]. Following deglaciation after ~18 cal. ka BP (calibrated radiocarbon thousands of years ago), ice-sheet configuration on Ulu Peninsula was similar to that of today by ~6 ka[9, 14]. During the Holocene, a 9.5-10 km readvance of Glacier IJR45 is documented by a large boulder train leading from the glacier to the prominent Brandy Bay Moraine[15, 16] (Figure 1c), poorly dated to 4–5 cal. ka BP on the basis of marine shells in reworked glaciomarine sediments beneath the moraine[15]. These reworked shells yield scattered ages, and as they are reworked and not *in situ*, provide only a maximum age for the readvance. Radiocarbon ages from lake sediments within the boulder train suggest the glacier receded by 1.5 ± 0.2 to 4.6 ± 0.2 cal. ka BP[17], although these should also be treated as maximum ages because the lake sediments are contaminated with older carbon from glacial meltwater[15].

Together, these data indicate a 10 km glacier readvance after ~4.8 cal. ka BP, and possibly younger. Ice-core temperature records on James Ross Island indicate that the period 2–5 cal. ka BP was ~0.5°C warmer than the 1961–1991 average[11]. It has been suggested that any glacier readvances at this time must therefore have been driven by precipitation[15]; these glaciers are therefore presumably more sensitive to precipitation than air temperature, which has implications for future glacier behaviour in this region. However, this reconstructed Holocene glacier behaviour is contrary to the currently observed glacier recession and ice-shelf collapse with extensive summer melting[12] under contemporary warming[5].

The small cirque glaciers on Ulu Peninsula today are surrounded by steep, unstable, ice-cored moraines that are inferred to have formed within the last few centuries[18]. The moraines were formed by shearing and thrusting within the glacier snout, with shearing and deformation of subglacial debris, suggesting polythermal glacial processes. Since the formation of these moraines, the glaciers have receded by more than 100 m and thinned by 15-20 m[18]. The small cirque glaciers are now largely cold-based, meaning a change in thermal regime has occurred as they thinned (*ibid.*).

2. Climatic input data

2.1 Modern climate data

Climate data are sparse on the northern Antarctic Peninsula. Mean annual air temperatures range from -14.4°C at the summit of Mount Haddington[11, 19] to -4.8°C at Esperanza[20, 21]. The mean annual air temperature at Mendel Base is -7.2°C[4]. James Ross Island has 200-300 positive degree days per year (PDD)[22], with a trend for increasing positive degree days. Average accumulation on Glacier IJR45 from 2009-2010 was 0.65 m[23], with a slight seasonal bias meaning that more precipitation falls in the summer[19]. The wet adiabatic lapse rate for James Ross Island is -0.58°C per 100 m[24]. Values for sea-surface temperatures in the Weddell Sea range from -1.8°C[25] to -1.0°C[26], but are poorly constrained; a value of -1.6°C was used in model

implementation. The environmental forcing parameters used for model implementation are presented in Supplementary Table S1.

Supplementary Table S1. Model tuned and observed glaciological and environmental bounding conditions for glacier IJR45 on Ulu Peninsula, James Ross Island. *Poorly constrained data.

Parameter	Observed value	Units
Mean annual air temperature at sea level[4]	-7.2	°C
Temperature lapse rate[24]	-0.0058	$ma^{-1} m^{-1}$
Precipitation lapse rate*[1, 3, 4, 23]	0.0002292	$ma^{-1} m^{-1}$
Mean annual precipitation[1]	0.65	$m\ a^{-1}$
Sea surface temperature*	-1.6	°C
Temperature range*[1, 3, 4, 23]	20	°C
Geothermal heat flux[27, 28]	69	$mW\ m^{-2}$
Day of maximum temperature	1st January	-
Day of maximum precipitation	1st March	-
Seasonal difference in precipitation*[19]	40% difference-to-mean between minimum and maximum precipitation	-

2.2 Holocene climate data

Holocene climate data are available from the recently acquired James Ross Island ice core from the summit of Mount Haddington[11, 12, 19]. This ice core provides temperature reconstructions at 10 and at 100 year resolution from 14 cal. ka BP to present. A lateral-flow and thinning-corrected accumulation record is available from this ice core from 1807-2007 AD, provided by Dr Nerilie Abram (Pers. comm.). The chronology is based on annual cycle of nss-SO_4, as well as volcanic tie points including the 1809/1815 volcanic eruption fixed points. To account for down-core thinning, a basic Nye thinning factor has been applied. This ice-core record shows no long-term trend in accumulation at the James Ross Island site over the past 200 years. This core updates previous accumulation records from this site[29, 30, 31] (annual means).

2.3 Future climate data

Future transient runs were forced by a regional atmospheric climate model with a multi-layer snow module (RACMO2), forced at the lateral boundaries by global climate model (GCM) data[32, 33]. Two different GCMs are used: ECHAM5 and HadCM3, run until 2100 AD (ECHAM5) and 2200 AD (HadCM3) under two different International Panel on Climate Change (IPCC) emission scenarios (A1B and E1), in order to capture a realistic range of future climate states. The A1B and E1 projections correspond to a middle-of-the-road and aggressive mitigation strategies respectively. Both HadCM3 and ECHAM5 simulations have a cold bias in the Antarctic Peninsula, compared with *in situ* temperature observations and ice-core records (See Evaluation of RACMO2 climate forcing, below), similar to that found for the entire Antarctic Ice Sheet[32].

The RACMO2 simulations for this grid cell are at 55 km resolution, and include two-metre air temperature and precipitation projections. The grid point coordinates used are 63.83°S and 58.02°W, a grid point that is 60% land and 40% sea, which is realistic considering the surroundings of James Ross Island. Because there is a cold bias in the GCM-forced RACMO2 simulations, we correct this bias against a RACMO2 benchmark simulation forced by ERA-40 reanalysis, which we treat as 'reality' for the period 1980-1999. Future temperature anomalies are calculated in relation to the average over the contemporary climate (1980-1999). In order to avoid difficulties arising from white noise in the annual data[34], the glacier model is then forced with 10-year climatic means of two-metre air temperature and precipitation. Four scenarios of

future air temperature and precipitation data (ECHAM5 and HadCM3, both for the IPCC A1B and E1 scenarios) are therefore used to investigate future response of IJR45 to climate change (Figure 4c, d, e in the main manuscript).

3. Evaluation of RACMO2 climate forcing

RACMO2 has been shown to realistically simulate the Antarctic near-surface climate[35, 36] and surface mass balance[37, 38, 39], including low SMB areas[40, 41], surface melt extent and magnitude[42, 43] and accumulation variability in Dronning Maud Land[44] and West Antarctica[45]. Compared with these regions, the Antarctic Peninsula, and James Ross Island in particular, experience a relatively wet and mild climate. Here, we evaluate the RACMO2 simulation for James Ross Island by comparing simulated 2-m air temperatures with observations from the nearby Marambio station (data from the READER dataset; ref. [46]) and with accumulation records from several ice cores from the Antarctic Peninsula region.

3.1 2-m air temperature

Table S2 shows the average 2-m air temperature and the standard deviation (as a measure for inter-annual variability) over the period 1980-1999 for Marambio station (64.2°S, 56.7°W) and the three RACMO2 contemporary (1989–1999) climate simulations; R-ERA, R-HadCM3 and R-ECHAM5. The values of the closest RACMO2 land grid point (64.3°S, 57.6°W) were chosen to be representative. R-ERA is laterally forced by ERA-40 re-analysis data, while the other two are laterally forced by Global Climate Model (GCM) output. Only the average and inter-annual variability are compared, as the GCM-forcings represent climate simulations.

Supplementary Table S2. Annual average 2-m air temperature over the period 1980-1999 for Marambio station and three RACMO2 simulations (R-ERA, R-HadCM3 and R-ECHAM5). Also the standard deviation of the average is provided, as well as the surface elevation.

	Mean annual air temperature	Standard deviation	Surface Elevation
Marambio	-8.4 °C	1.22 °C	198 m
R-ERA	-8.8 °C	1.26 °C	327 m
R-HadCM3	-10.6 °C	1.08 °C	327 m
R-ECHAM5	-10.1 °C	1.26 °C	327 m

The average temperature and inter-annual variability between R-ERA and the observations agree well, with the lower average temperature in RACMO2 partly caused by the higher surface elevation of the RACMO2 grid point (327 m versus 198 m). The two GCM-forced RACMO2 simulations show lower temperatures as was also found for the remainder of the Antarctic ice sheet[32]. This cold bias probably arises from lower sea-surface temperatures and subsequent higher sea-ice cover extent. In the contemporary and future GCM-forced simulations, this cold bias in near-surface temperature was removed.

The READER dataset contains more temperature records from station across the Antarctic Peninsula, but these were not used, as 1) most stations are located on the western side of the AP, which has a different climate than the east side, where James Ross Island is situated, 2) the stations are located at sea level in the vicinity of the ocean making it difficult to compare with either RACMO land or sea grid points, or 3) substantial data was missing for the 1980-1999 period.

For the calculation of future summer melt in the glacier model, the simulated seasonal cycle in near-surface temperature is important. Figure S1 shows the seasonal temperature cycle as observed at Marambio station and as simulated in the three RACMO2 simulations. R-ERA again shows the best agreement. The modelled temperatures are slightly higher in autumn and slightly lower in spring and summer, probably caused by differences in sea-ice cover and extent. The GCM-forced RACMO2 simulations show lower temperatures especially in winter and spring. When the 2-m temperature of these simulations is bias-corrected, summer temperatures agree very well with the observations, ensuring that the correct amount of summer melt is obtained by the degree-day model.
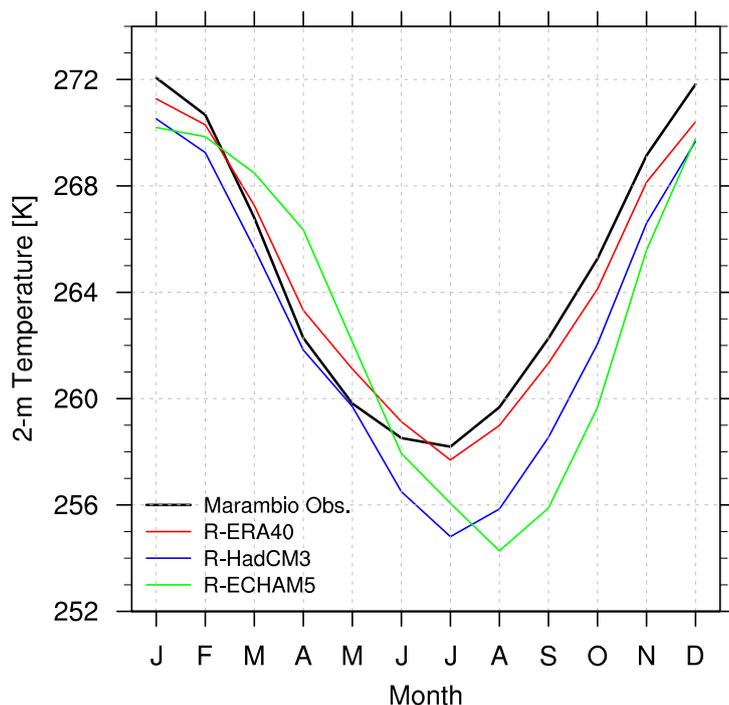
Supplementary Figure 1. *Average (1980-1999) seasonal cycle in 2-meter air temperature as observed at Marambio station (black) and as simulated by three RACMO2 simulations; R-ERA (red), R-HadCM3(blue) and R-ECHAM5 (green).*

3.2 Accumulation

Table S3 shows the climatic average accumulation for three Antarctic Peninsula ice cores; Gomez[30], Dyer Plateau[47], and James Ross Island[29], and the values from three RACMO2 simulations; R-ERA, R-HadCM3, and R-ECHAM5. The value of the closest RACMO2 land grid point is chosen to be representative. Given the complex topographic setting and the large climatic gradients in this area, the modelled accumulation rates agree well with the observations, although the inter-annual variability at both Dyer Plateau and James Ross Island is underestimated. The small difference between R-ERA and the GCM-forced simulations at James Ross Island results in a small bias correction on the accumulation rates.

		Gomez	Dyer Plateau	James Ross Island
Location	**Latitude**	73.6°S	70.4°S	64.2°S
	Longitude	70.4°W	64.5°W	57.7°W
Average annual Accumulation (kg m²)	**Ice core**	894[1] ± 200 (average 1960-2006)	474[2] ± 137 (average 1960-1988)	659[3] ± 193 (average 1960-1997)
	R-ERA	1188 ± 247	375 ± 67	559 ± 76
	R-HadCM3	701 ± 165	229 ± 48	606 ± 104
	R-ECHAM5	925 ± 226	323 ± 79	538 ± 80

The difference in future precipitation change between ECHAM5 and HadCM3 is likely to be a function of a local change in the sea ice concentration and sea surface temperatures in either of the two GCMs. Over the entire Antarctic Ice Sheet, and a major part of the Antarctic Peninsula, a uniform increase in snowfall is simulated (see Figure 10b in ref. [32]). This is in agreement with previous studies[48, 49, 50, 51, 52], where it is found that precipitation scales more or less linearly with increasing temperature (approximately a 5% increase per degree of temperature increase), indicating that the increase in air temperature is the major driver of precipitation change, rather than changes in atmospheric circulation. On the Antarctic Peninsula, the change in future precipitation is also correlated with a change in sea-ice extent. However, GCMs are not currently capable of realistically simulating change in future sea-ice cover and concentration. Although the four simulations differ with respect to precipitation change, they do agree on future temperature increase and glacier recession, therefore strengthening the conclusions of the paper that Glacier IJR45 is mainly influenced by temperature (i.e., melt) changes than precipitation changes.

4. Numerical model description

We used a one dimensional finite difference ice sheet flowline model with a 100 m horizontal resolution (previously described in refs. [53, 54]), which uses a forward explicit numerical scheme implemented over a staggered grid that spans the length and foreland of IJR45, projecting into Prince Gustav Channel (Figure 1 in main manuscript). The model accounts for the dynamic effects exerted by longitudinal stresses by incorporating a triangular averaging filter that smooths gravitational driving stress values and velocities that arise from them. Horizontal flux is calculated as the product of the cross-sectional planar area described by a symmetrical trapezoid, and the vertically-averaged centreline ice velocity. Calculation of this latter term incorporates a width-dependent shape factor that uses tabulated values[55] for a parabolic glacier cross-profile[54] to adjust centreline velocities in areas where valley-side drag is expected to exert greatest influence. Incorporation of the width term in the flux equation ensures that mass is conserved in areas where the valley width changes, by producing faster or slower flow.

The model includes a flow enhancement coefficient (*E*), which accounts for the softening of the ice by impurities or contrasts in crystal orientation (Table S4). Sliding is governed by an exponential function,

allowing sliding to occur over a range of temperatures close to the pressure melting point. Mass balance and climate boundary conditions are derived from point observations of mean annual air temperature and precipitation (Table S1). Daily surface temperatures and precipitation volumes are determined from a simple cosine function constrained by an annual temperature / precipitation range that calculates deviation from an annual mean[54] (Supplementary Figure 2). A positive degree-day scheme, similar to that used by ref. [56], is then used to calculate surface melting. As these data are not available from observations, the degree-day factors are tuned during model parameterisation. Refreezing, the rain/snow threshold, and the seasonality distribution (amplitude and timing) of precipitation are also controlled by the scheme. Annual precipitation is assumed to equal surface accumulation if temperatures are below 1°C. Above this threshold, it is assumed to fall as rain and is lost to the system. The range of daily temperatures and precipitations calculated by the positive degree day scheme are illustrated in Supplementary Figure 2. Calving and basal melting calculations for the marine-terminating part of the glacier follow ref. [57].

Supplementary Table S4. Physical and model constants (after Golledge and Levy, 2011). Tuned parameters are indicated with a * symbol.

| Parameter (and reference for values)	Value	Units
Density of ice	920	kg m^{-3}
Density of sea water	1028	kg m^{-3}
Density of mantle	3300	kg m^{-3}
Gravitational acceleration	9.81	m s^{-2}
Glen's flow law exponent	3	-
Sliding rate factor*	6.00e-08	-
Sliding exponent	3	-
Flow enhancement factor*	9	-
Thermal parameter ($T \geq 263.15$ *K*)	5.47e-10	-
Thermal parameter ($T \geq 263.15$ *K*)	1.14e-5	-
Till thickness limiting bedrock erosion	2	M
Universal gas constant	8.314	J mol^{-1} K^{-1}
Degree-day factor (ice)*	0.009	m yr^{-1}
Degree-day factor (snow)*	0.009	m yr^{-1}
Snow-rain threshold*	1	°C
Temperature range*	21.5	°C
Thermal conductivity of ice	204	W m^{-1} K^{-1}
Lithospheric relaxation time	3000	Yr
Horizontal domain resolution	100	M
Valley side angle	45	°
Creep activation energy	139 or 60	kJ mol^{-1}
Calving constant*	0.25	-
Precipitation lapse rate*	0	ma^{-1} m^{-1}
Refreezing*	0	-
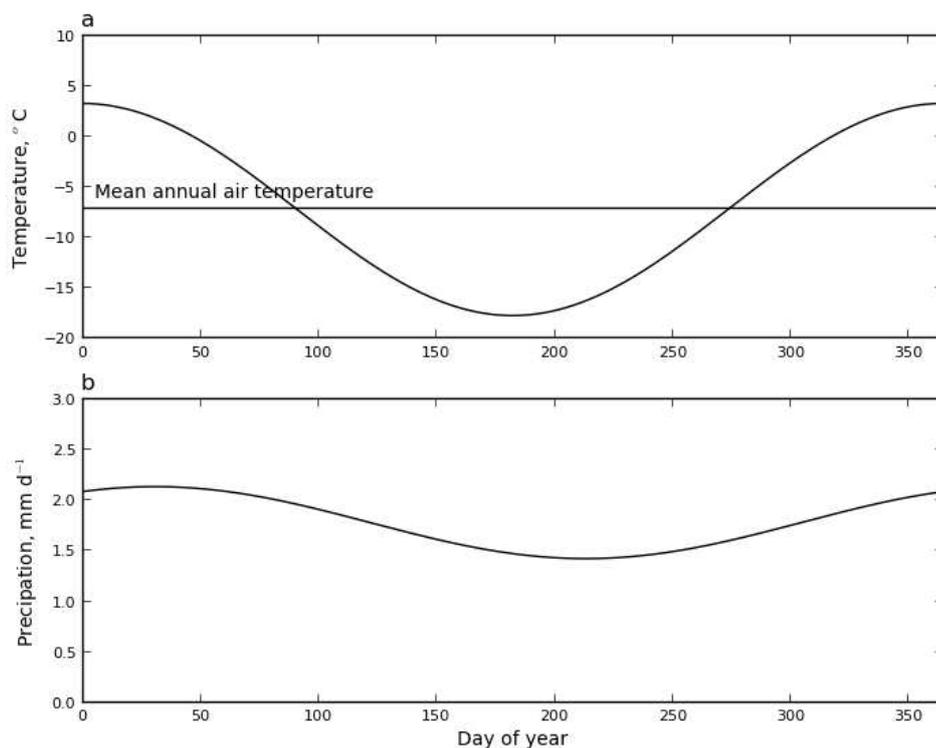
Supplementary Figure 2. Climate seasonality as calculated by the model. Temperature range and precipitation range are derived from observations. The amplitude of precipitation variability (40%) is calculated as a difference from the annual mean. The mean annual air temperature (-7.2°C) is denoted by the straight line in plot 'a'.

5. Numerical modelling strategy

5.1 Model parameterisation and dynamic calibration

The model's flowline was placed along the centreline of a reconstructed flow unit for the large Holocene readvance (Figure 1c, d), and projects forwards into Prince Gustav Channel. Accumulation areas were inferred on Lachman Crags, but Johnson Mesa was left ice-free, as published cosmogenic nuclide ages suggest that this area deglaciated around 8 ka[9]. Davies Dome was also inferred not to have contributed ice, on the basis of the presence of LGM-age basalt boulders in the ice dome's foreground[14].

Our modelling strategy is outlined in Supplementary Figure 3. Our model parameterisation used observational data and then tuned parameters until the glacier replicated observed velocity, ice-surface elevation, volume and length as closely as possible. This assumed that the glacier is in equilibrium. We then performed a dynamic calibration[58], a series of short transient runs from 1850-present (the period when accumulation and temperature data are available from the James Ross Island ice-core record[11, 12, 19, 30]), where the glacier parameters are modified until the glacier replicates observed rates of glacier recession[1] over the last 30 years as closely as possible. The glacier was thus calibrated and validated against the historical record of glacier length (cf. ref. [59]).
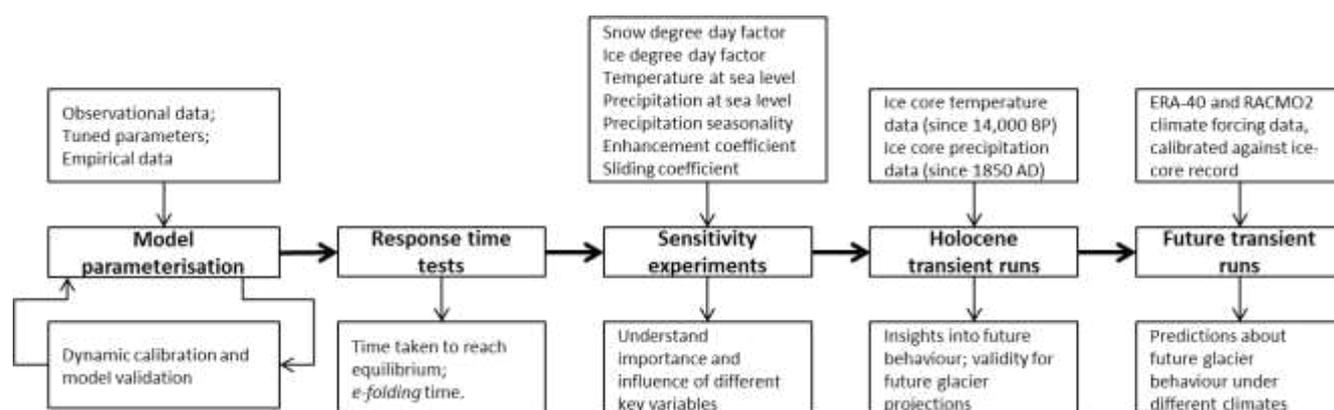
Supplementary Figure 3. Flow chart outlining and summarising the modelling strategy.

5.2 Response time tests

Response-time tests and sensitivity tests were undertaken on the dynamically calibrated glacier in order to understand how the model reacts to model parameterisation and climate variability, and to test the influence of poorly known model parameters, such as the enhancement factor (cf. ref. [60]). The response-time tests (15 experiments) assessed perturbations from a control point; tests were run on the equilibrium glacier and were run to equilibrium. Response time tests assessed the time taken for the glacier to reach equilibrium following a temperature perturbation (from +1.0°C to -0.5°C in 0.1°C increments). Response time tests were limited by the non-linear response of the glacier to cooling beyond -0.5°C, when it begins to calve. The *e-folding* time, the time taken for the glacier to achieve two-thirds of its volume response, was also calculated (cf. refs. [61, 62, 63]).
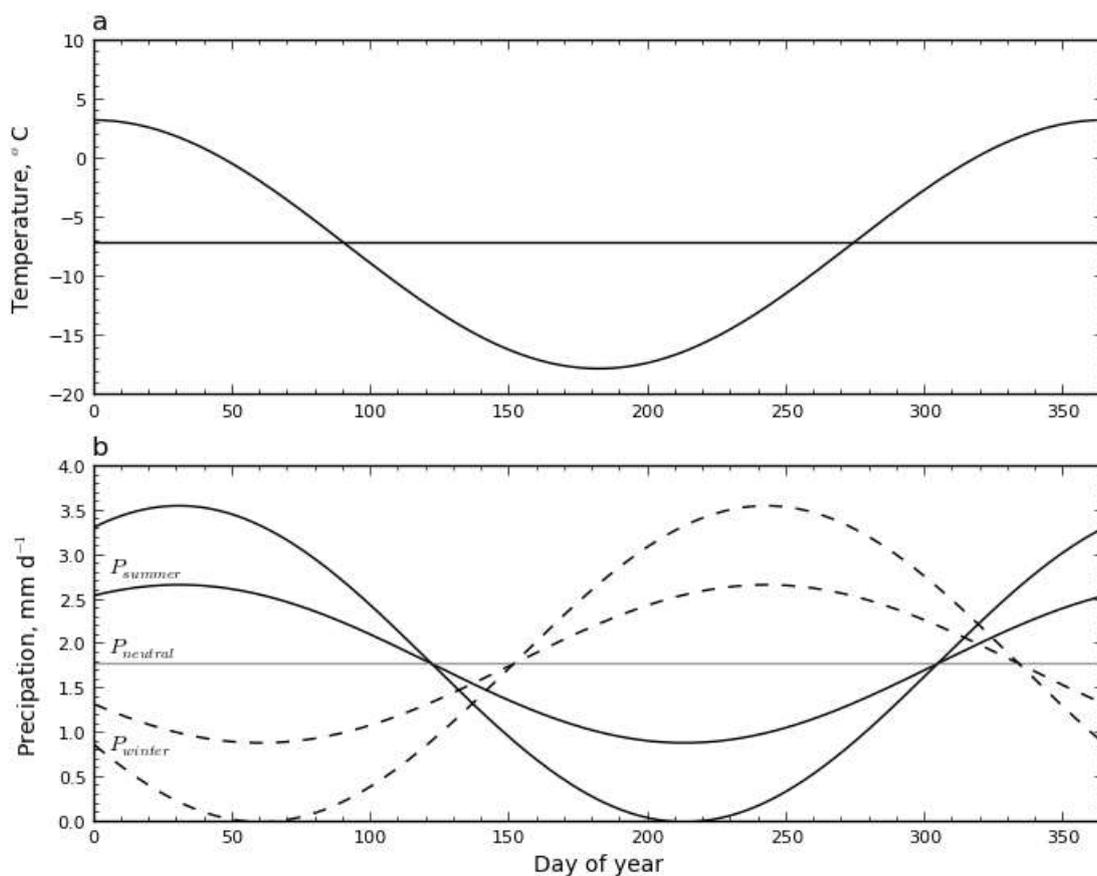
5.3 Sensitivity experiments

We tested the sensitivity of the glacier to perturbations in key model and climate parameters (Supplementary Figure 3): the snow and ice degree-day factors (both ±20% in 0.0001 increments, 31 experiments each), temperature (from -1.5°C to +2°C in 0.1°C increments, which covers the range of temperatures experienced during the Holocene and projected for the next 200 years; 35 experiments) and precipitation (±20% in 0.01 m increments; 31 experiments), the flow enhancement coefficient (0 to 10 in 0.5 increments; 21 experiments) and the sliding coefficient (±20% in 2e-10 increments; 12 experiments). Each sensitivity test was run to equilibrium and imposes a small incremental change to the parameter in question. We also analysed the effect of changing precipitation and temperature synchronously, through a Monte-Carlo style analysis (558 experiments).

Precipitation seasonality is a key variable, as it can exert significant controls on glacier mass balance[56]. Precipitation during summer could fall as rain (which, in our model, is considered lost to the system), but can also decrease fresh snow, reduce the glacier surface albedo, and result in greater ablation from the glacier surface[64]. Conversely, winter precipitation may build up a reservoir. Warming on summer-accumulation type glaciers therefore causes a significant decrease in snow accumulation, decreases the surface albedo and prolongs the melt season. However, warming on winter-accumulation type glaciers prolongs the melt season without changing snowfall in summer[65]. Because Glacier IJR45 exists in a region with a summer-accumulation climate pattern[19], and because future increases in precipitation are projected to largely occur in the summer months[50], it is meaningful to evaluate the effect of precipitation seasonality on Glacier IJR45.

We conducted two experiments, each comprising 41 simulations, under contrasting precipitation patterns: a sinusoidal pattern in-phase with temperature ("P$_{summer}$") and anti-phased with temperature ("P$_{winter}$"). All other parameters were held constant. For each precipitation seasonality regime, the amplitude of the sinusoid of precipitation variability was set from 0% (where precipitation is evenly distributed throughout the year; P$_{neutral}$) to 200% (where precipitation reaches zero at its minimum) in 5% increments (Supplementary Figure 4).

We also conducted an experiment to investigate how important the amplitude of summer precipitation seasonality is at different mean annual air temperatures. We therefore changed mean annual air temperature (-8°C to -5.4°C in 0.2°C increments) and amplitude of summer precipitation seasonality simultaneously (0 to 200% in 20% increments) (176 experiments).

Supplementary Figure 4. Contrasting precipitation regimes for seasonality sensitivity experiments. For P$_{summer}$ (solid black line) and P$_{winter}$ (dashed black line), the amplitude of the sinusoid varied from 0% (P$_{neutral}$ in the figure above) to 200%, where precipitation reaches 0 mm d^{-1} at its minimum. Amplitudes of 0%, 100% and 200% are shown in the figure above. Under summer precipitation experiments, the 60th day of the year (1st March) receives the most precipitation, in line with observations[19]. Under winter precipitation experiments, the 213th day of the year is set to receive the most precipitation.

5.4 Transient simulations

Subsequent transient runs used the James Ross Island ice core record to force glacier fluctuations through the Holocene. The ice-core record provides a high-resolution temperature record over the last 14,000 years[11], but precipitation data are only available from this ice core since 1807[12]. Forcing data for this

period is available at 10-year resolution, and this captures glacier response to Twentieth-Century warming. Prior to this the glacier is forced with 100-year resolution data.

There are no accumulation data prior to 1807, so for transient runs before this time, we forced the precipitation to vary with temperature (7 experiments). Runs occurred with precipitation held constant at modern values (0.65 m a^{-1}), and also forced by a 5%, 7.3% (the generally held value for precipitation variance with temperature, cf. ref [66]), 15%, 20% and 100% increase for every 1°C rise in temperature, in order to explore a range of possible climate scenarios. All other values (sea-surface temperature, precipitation and temperature lapse rates, degree-day factors, geothermal heat flux and calving coefficient) were held constant at modern observed or tuned values.

Future scenarios were forced from 1850 AD through to 2200 AD. From 1850 until 2010 the glacier was forced with observed temperature and accumulation data from the James Ross Island ice core record. From 2010 until 2200 AD, the glacier was forced with the calibrated and bias-corrected RACMO2 dataset (4 experiments). This approach ensured that the future scenarios were as realistic as possible.

6. Results

6.1 Model parameterisation and dynamic calibration

We used observed glaciological, climatic and environmental variables to initialise the model (Table S1). Flow parameters and unknown variables (degree-day factors for ice and snow, calving flux, sliding and flow enhancement coefficients [the deformation factor]) were tuned to provide a close fit to observed glacier geometry, flow velocity, ice thickness and volume. Given these parameters, our modelled glacier stabilised and reached equilibrium within 100 years, has a maximum flow velocity of 6.22m a^{-1}. The majority of the velocity derives from the ice deformation component.

Small changes were required for the annual temperature range and precipitation lapse rate during tuning. Other environmental and climatic parameters are as observed (Table S1). The annual temperature range was revised from 20°C to 21.5°C. Precipitation has been measured as 0.65 m per annum at both the summit of IJR45 and at the summit of Mount Haddington. Poorly-constrained and short-term measurements from Mendel Base, at sea level, estimate annual precipitation to b 0.3 m per annum. The precipitation lapse rate results in a very skewed glacier, with extreme precipitation gradients. Given the low altitudinal range and profile of our glacier and the low confidence in precipitation measurements, we therefore assume a lapse rate of 0 and distribute precipitation evenly across the glacier surface. This simplification is unlikely to have a significant effect on our results as our study shows that large changes in precipitation have little effect on this glacier. Decreasing the amount of precipitation falling onto the ablation area would only amplify this response and would not affect the study's findings.

We then perform a dynamic calibration using observed temperature and accumulation over the last 160 years from the ice-core record (using 10 year means, the highest available resolution for temperature data). Small adjustments were made to the flow parameters and degree day factors until the glacier replicated observed rates of glacier recession and volume change from 1979-2006 (cf. ref [1]). The glacier stabilises in a position that matches present-day glacier geometry, volume and velocity well, although it is slightly shorter than the observed glacier from measurements taken in 2006 (ref [1]) (Table S5).

Graphical outputs from the dynamic calibration are presented in Supplementary Figure 5, and a comparison to the modern glacier is presented in Supplementary Figure 6. Therefore, following a 160 year
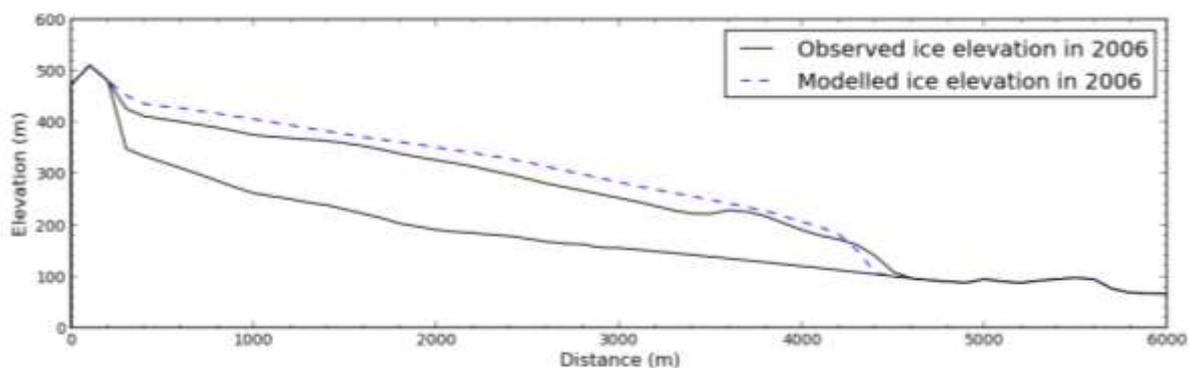
transient run with temperature and precipitation forced by the ice-core record, the modelled glacier not only achieves an excellent fit to observed historic rates of recession and volume change, but also to observed geometry and velocity. These observations validate our glacier model, showing that it performs well over historical timescales.

Supplementary Table S5. Model tuning results at the end of dynamic calibration (comparison to observations from 2006). Modelled rates of change are within errors of observations. Rates of volume and surface area change are from ref. s[1].

| Parameter	Modelled (2006)	Observed (2006)
Deformation velocity component (m^{-1} a^{-1})	6.14	-
Sliding velocity component (m^{-1} a^{-1})	0.02	-
Maximum velocity (m^{-1} a^{-1})	6.16	7.1
Volume (km^3)	0.5304	0.4385
Length (m)	4200	4400
Surface area (km^2)	5.252	5.356
Equilibrium line altitude (m a.s.l.)	306	271[5]
Rate of glacier volume change (km^3 a^{-1}) from 1979-2006	0.00103	0.001 ± 0.001
Rate of glacier surface area change (km^2 a^{-1}) from 1979-2006	0.0048	0.011 ± 0.001
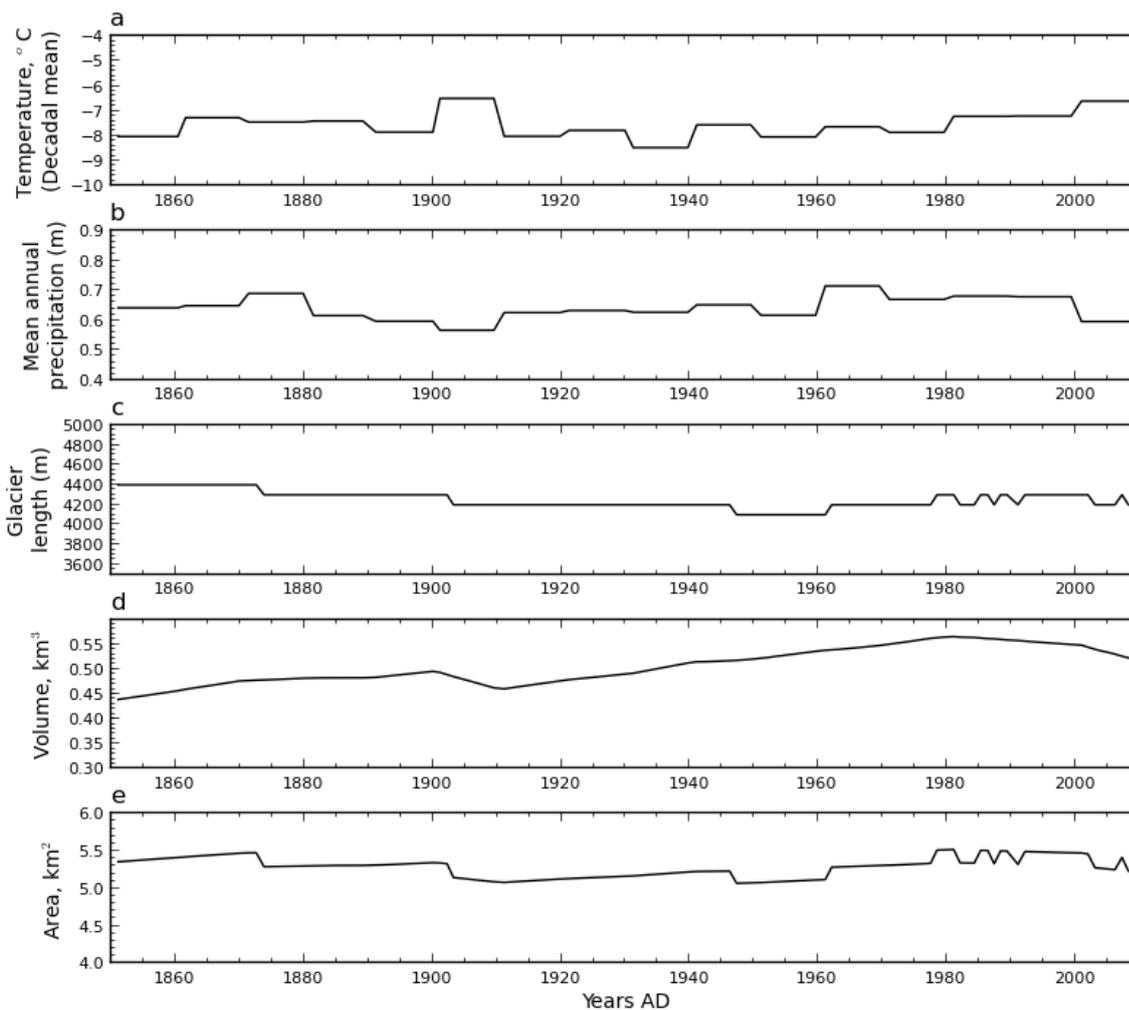
Supplementary Figure 5. Results of the dynamic calibration of our glacier model, showing that it replicates observed recession in the 1980s-early 2000s, followed by stabilisation at its current position. Decadal temperature and precipitation means from 1850-2010 are derived from the ice-core record[11, 19, 29].

Supplementary Figure 6. Results of dynamic calibration in the year 2010 AD, showing a good fit of the glacier's modern geometry after a 160 year run with temperature and precipitation forced by the ice-core record. Dashed black line is observed glacier surface. Blue line is the modelled glacier surface following dynamic calibration.

6.2 Sensitivity experiments

Results of the sensitivity experiments are presented in full in Supplementary Figure 7. Changes to the basal sliding coefficient yielded little change, so these data are not shown. It is instantly clear that temperature, and then precipitation, has the greatest effect on glacier length, volume and velocity.
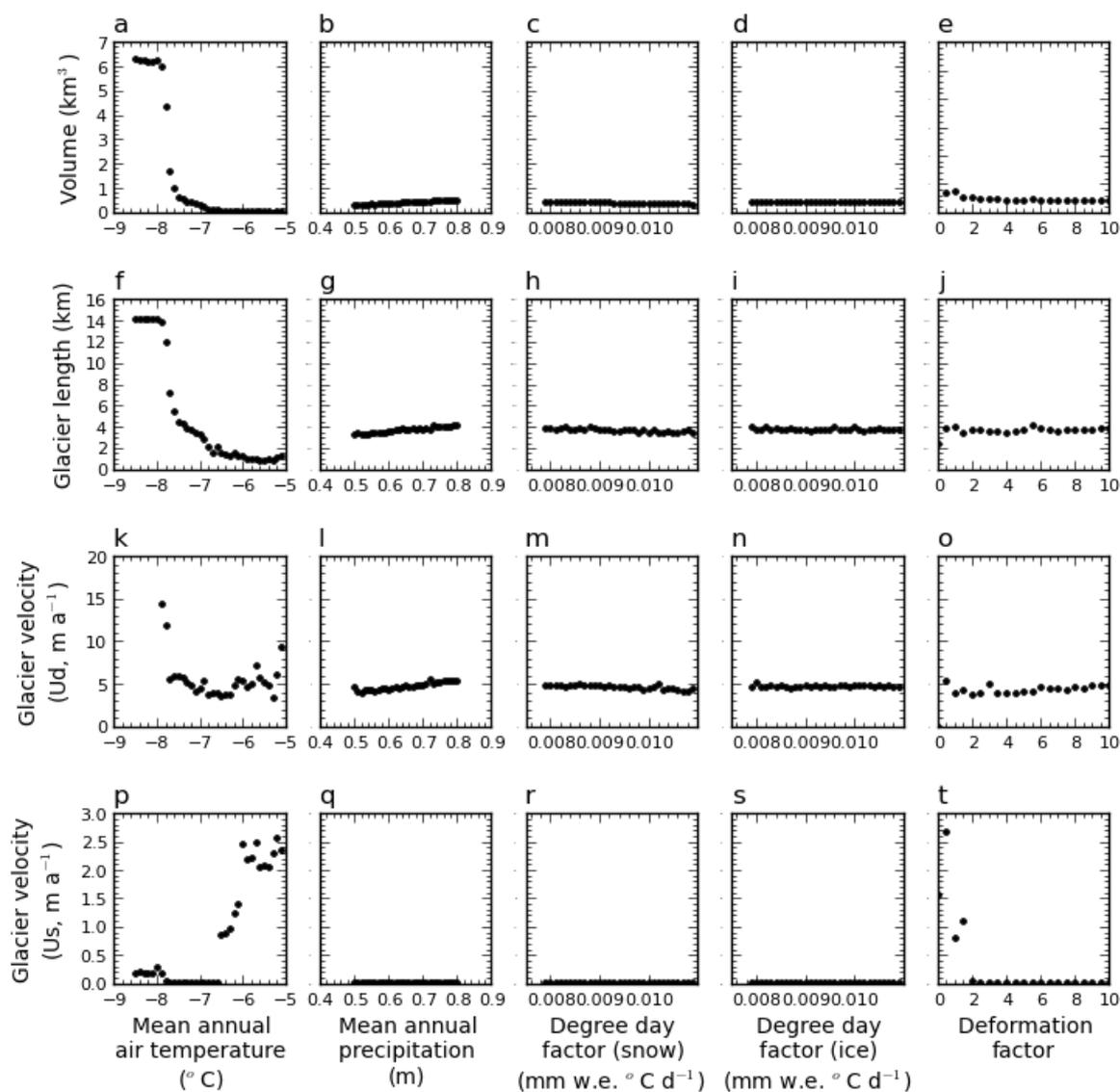
Supplementary Figure 7. Results of sensitivity experiments, with the change in glacier volume (a-e), length (f-j), and velocity arising from the deformation component (k-l) and the sliding component (p-t) (both domain maximum). Each experiment follows a perturbation to mean annual air temperature, precipitation, snow and ice degree day factors and flow enhancement coefficient (ice deformation factor).

7. References

1.   Engel Z, Nývlt D, Láska K. Ice thickness, areal and volumetric changes of Davies Dome and Whisky Glacier in 1979-2006 (James Ross Island, Antarctic Peninsula). *Journal of Glaciology* 2012, **58**(211)**:** 904-914.

2.   Nývlt D, Šerák L. James Ross Island - Northern Part. Topographic Map 1:25 000. Praha: Czech Geological Survey; 2009.

3.   Laska K, Nyvlt D, Engel Z, Budìk L. Seasonal variation of meterological variables and recent surface ablation / accumulation rates on Davies Domes and Whisky Glacier, James Ross Island, Antarctica. *Geophysical Research Abstracts* 2012, **14**: EGU2012-5545.

4.   Laska K, Prosek P, Budik L. Seasonal variation of air temperature at the Mendel Station, James Ross Island, in the period of 2006-2006. *Geophysical Research Abstracts* 2010, **12:** EGU2010-3880.

5.   Davies BJ, Carrivick JL, Glasser NF, Hambrey MJ, Smellie JL. Variable glacier response to atmospheric warming, northern Antarctic Peninsula, 1988–2009. *The Cryosphere* 2012, **6:** 1031-1048.

6.   Glasser NF, Scambos TA, Bohlander JA, Truffer M, Pettit EC, Davies BJ. From ice-shelf tributary to tidewater glacier: continued rapid glacier recession, acceleration and thinning of Röhss Glacier following the 1995 collapse of the Prince Gustav Ice Shelf on the Antarctic Peninsula. *Journal of Glaciology* 2011, **57**(203)**:** 397-406.

7.   Cooper APR. Historical observations of Prince Gustav Ice Shelf. *Polar Record* 1997, **33**(187)**:** 285-294.

8.   Cook AJ, Vaughan DG. Overview of areal changes of the ice shelves on the Antarctic Peninsula over the past 50 years. *The Cryosphere* 2010, **4**(1)**:** 77-98.

9.   Johnson JS, Bentley MJ, Roberts SJ, Binney SA, Freeman SPHT. Holocene deglacial history of the north east Antarctic Peninsula - a review and new chronological constraints. *Quaternary Science Reviews* 2011, **30**(27-28)**:** 3791-3802.

10.   Pudsey CJ, Murray JW, Appleby P, Evans J. Ice shelf history from petrographic and foraminiferal evidence, Northeast Antarctic Peninsula. *Quaternary Science Reviews* 2006, **25**(17-18)**:** 2357-2379.

11.   Mulvaney R, Abram NJ, Hindmarsh RCA, Arrowsmith C, Fleet L, Triest J*, et al.* Recent Antarctic Peninsula warming relative to Holocene climate and ice-shelf history. *Nature* 2012, **489:** 141-144.

12.   Abram NJ, Mulvaney R, Wolff EW, Triest J, Kipfstuhl S, Trusel LD*, et al.* Acceleration of snow melt in an Antarctic Peninsula ice core during the Twentieth Century. *Nature Geosci* 2013, **6:** 404-411.

13.   Scambos T, Fricker HA, Liu C-C, Bohlander J, Fastook J, Sargent A*, et al.* Ice shelf disintegration by plate bending and hydro-fracture: Satellite observations and model results of the 2008 Wilkins ice shelf break-ups. *Earth and Planetary Science Letters* 2009, **280**(1-4)**:** 51-60.

14.   Glasser NF, Davies BJ, Carrivick JL, Rodés A, Hambrey MJ, Smellie JL*, et al.* Ice-stream initiation, duration and thinning on James Ross Island, northern Antarctic Peninsula. *Quaternary Science Reviews* 2014, **86:** 78-88.

15.   Hjort C, Ingólfsson Ó, Möller P, Lirio JM. Holocene glacial history and sea-level changes on James Ross Island, Antarctic Peninsula. *Journal of Quaternary Science* 1997, **12:** 259-273.

16.   Davies BJ, Glasser NF, Carrivick JL, Hambrey MJ, Smellie JL, Nývlt D. Landscape evolution and ice-sheet behaviour in a semi-arid polar environment: James Ross Island, NE Antarctic Peninsula. In: Hambrey MJ, Barker PF, Barrett PJ, Bowman VC, Davies BJ, Smellie JL*, et al.* (eds). *Antarctic Palaeoenvironments and Earth-Surface Processes*, vol. 381. Geological Society, London, Special Publications, volume 381: London, 2013, pp 353-395.

17. Björck S, Olsson S, Ellis-Evans C, Håkansson H, Humlum O, de Lirio JM. Late Holocene palaeoclimatic records from lake sediments on James Ross Island, Antarctica. *Palaeogeography, Palaeoclimatology, Palaeoecology* 1996, **121**(3-4)**:** 195-220.

18. Carrivick JL, Davies BJ, Glasser NF, Nývlt D, Hambrey MJ. Late Holocene changes in character and behaviour of land-terminating glaciers on James Ross Island, Antarctica. *Journal of Glaciology* 2012, **58**(212)**:** 1176-1190.

19. Abram NJ, Mulvaney R, Arrowsmith C. Environmental signals in a highly resolved ice core from James Ross Island, Antarctica. *Journal of Geophysical Research: Atmospheres* 2011, **116**(D20)**:** D20116.

20. Skvarca P, Rack W, Rott H, Donángelo T. Evidence of recent climatic warming on the eastern Antarctic Peninsula. *Annals of Glaciology* 1998, **27:** 628-632.

21. Stastna V. Spatio-temporal changes in surface air temperature in the region of the northern Antarctic Peninsula and south Shetland islands during 1950-2003. *Polar Science* 2010, **4**(1)**:** 18-33.

22. Barrand NE, Vaughan DG, Steiner N, Tedesco M, Kuipers Munneke P, van den Broeke MR*, et al.* Trends in Antarctic Peninsula surface melting conditions from observations and regional climate modeling. *Journal of Geophysical Research: Earth Surface* 2013, **118**(1)**:** 315-330.

23. Láska K, Nývlt D, Engel Z, Kopačková V. Meterological data and mass balance measurements on Davies Dome and Whisky Glacier in 2006-2010, James Ross Island, Antarctica. *Geophysical Research Abstracts* 2011, **13:** EGU2011-4858.

24. Aristarain AJ. Accumulation and temperature measurements on the James Ross Island ice cap, Antarctic Peninsula, Antarctica. *Journal of Glaciology* 1987, **33**(115)**:** 357-362.

25. Žarić S, Donner B, Fischer G, Mulitza S, Wefer G. Sensitivity of planktic foraminifera to sea surface temperature and export production as derived from sediment trap data. *Marine Micropaleontology* 2005, **55**(1–2)**:** 75-105.

26. Domack EW, Burnett A, Leventer A. Environmental setting of the Antarctic Peninsula. In: Domack E, Leventer A, Burnett A, Bindshadler R, Convey P, Kirby M (eds). *Antarctic Peninsula Climate Variability: Historical and Paleoenvironmental Perspectives*, vol. 79, 2003, pp 1-13.

27. Llubes M, Lanseau C, Rémy F. Relations between basal condition, subglacial hydrological networks and geothermal flux in Antarctica. *Earth and Planetary Science Letters* 2006, **241**(3–4)**:** 655-662.

28. Maule CF, Purucker ME, Olsen N, Mosegaard K. Heat Flux Anomalies in Antarctica Revealed by Satellite Magnetic Data. *Science* 2005, **309**(5733)**:** 464-467.

29. Aristarain A, Delmas R, Stievenard M. Ice-Core Study of the Link between Sea-Salt Aerosol, Sea-Ice Cover and Climate in the Antarctic Peninsula Area. *Climatic Change* 2004, **67:** 63-86.

30. Thomas ER, Marshall GJ, McConnell JR. A doubling in snow accumulation in the western Antarctic Peninsula since 1850. *Geophysical Research Letters* 2008, **35**(1)**:** L01706.

31.   Miles GM, Marshall GJ, McConnell JR, Aristarain AJ. Recent accumulation variability and change on the Antarctic Peninsula from the ERA40 reanalysis. *International Journal of Climatology* 2008, **28**(11)**:** 1409-1422.

32.   Ligtenberg SRM, van de Berg WJ, van den Broeke MR, Rae JGL, van Meijgaard E. Future surface mass balance of the Antarctic ice sheet and its influence on sea level change, simulated by a regional atmospheric climate model. *Climate Dynamics* 2013, **41**(3-4)**:** 867-884.

33.   Barrand NE, Hindmarsh RCA, Arthern R, Williams CR, Mouginot J, Scheuchl B*, et al.* Computing the volume response of the Antarctic Peninsula Ice Sheet to warming scenarios to 2200. *Journal of Glaciology* 2013, **59**(215)**:** 397-409.

34.   Roe GH. What do glaciers tell us about climate variability and climate change? *Journal of Glaciology* 2011, **57**(23)**:** 567-578.

35.   Lanaerts JTM, Van den Broeke MR. Modeling drifting snow in Antarctica with a regional climate model, Part II: Results. *Journal of Geophysical Research* 2012, **117:** D05109.

36.   Rodrigo JS, Buchlin J-M, Beeck Jv, Lenaerts JTM, Nroeke MRvd. Evaluation of the antarctic surface wind climate from ERA reanalyses and RACMO2/ANT simulations based on automatic weather stations. *Climate Dynamics* 2013, **40:** 353-376.

37.   van de Berg WJ, van den Broeke MR, Reijmer CH, van Meijgaard E. Reassessment of the Antarctic surface mass balance using calibrated output of a regional atmospheric climate model. *Journal of Geophysical Research: Atmospheres* 2006, **111**(D11)**:** n/a-n/a.

38.   Lenaerts JTM, van den Broeke MR, van de Berg WJ, van Meijgaard E, Kuipers Munneke P. A new, high-resolution surface mass balance map of Antarctica (1979–2010) based on regional atmospheric climate modeling. *Geophysical Research Letters* 2012, **39**(4)**:** L04501.

39.   Shepherd A, Ivins ER, A G, Barletta VR, Bentley MJ, Bettadpur S*, et al.* A Reconciled Estimate of Ice-Sheet Mass Balance. *Science* 2012, **338**(6111)**:** 1183-1189.

40.   Scambos TA, Frezzotti M, Haran T, Bohlander J, Lenaerts JTM, Broeke MRvd*, et al.* Extent of low-accumulation 'wind glaze' areas on the East Antarctic plateau: implications for continental ice mass balance. *Journal of Glaciology* 2012, **58**(210)**:** 633-647.

41.   Das I, Bell RE, Scambos TE, Wolovick M, Creyts TT, Studinger M*, et al.* Influence of persistent wind-scour on surface mass balance of Antarctica. *Nature Geoscience* 2013, **6:** 367-371.

42.   Kuipers Munneke P, Picard G, van den Broeke MR, Lenaerts JTM, van Meijgaard E. Insignificant change in Antarctic snowmelt volume since 1979. *Geophysical Research Letters* 2012, **39:** L01501.

43.   Trusel LD, Frey KE, Das SB, Kuipers Munneke P, van den Broeke MR. Satellite-based estimates of Antarctic surface meltwater fluxes. *Geophysical Research Letters* 2013, **40:** 6148-6153.

44.   Horwath M, Legresy B, Remy F, Blarel F, Lemoine J-M. Consistent patterns of Antarctic ice sheet interannual variations from ENVISAT radar altimetry and GRACE satellite gravimetry. *Geophysical Journal International* 2012, **189**.

45.   Medley B, Joughin I, Das SB, Steig EJ, Conway H, Gogineni S*, et al.* Airborne-radar and ice-core observations of annual snow accumulation over Thwaites Glacier, West Antarctica confirm the spatiotemporal variability of global and regional atmospheric models. *Geophysical Research Letters* 2013, **40:** 1-6.

46.   Turner J, Colwell SR, Marshall GJ, Lachilan-Cope TA, Carleton AM, Jones PD*, et al.* The SCAR READER Project: toward a high-quality database of mean Antarctic meteorological observations. *Journal of Climate* 2004, **17**(14)**:** 2890-2898.

47.   Thompson LG, Peel D, Mosley-Thompson E, Mulvaney R, Dal J, Lin P*, et al.* Climate since AD 1510 on Dyer Plateau, Antarctic Peninsula: Evidence for recent climate change. *Annals of Glaciology* 1994, **20**(1)**:** 420-426.

48.   Agosta C, Favier V, Krinner G, Gallée H, Fettweis X, Genthon C. High-resolution modelling of the Antarctic surface mass balance, application for the twentieth, twenty first and twenty second centuries. *Climate Dynamics* 2013, **41**(11-12)**:** 3247-3260.

49.   Lipzig NPM, van Meijgaard E, Oerlemans J. Temperature sensitivity of the Antarctic surface mass balance in a regional atmospheric climate model. *Journal of Climate* 2002, **15:** 2758-2774.

50.   Krinner G, Magand O, Simmonds I, Genthon C, Dufresne JL. Simulated Antarctic precipitation and surface mass balance at the end of the twentieth and twenty-first centuries. *Climate Dynamics* 2007, **28**(2-3)**:** 215-230.

51.   Bengtsson L, Koumoutsaris S, Hodges K. Large-scale surface mass balance of ice sheets from a comprehensive atmospheric model. *Surv Geophys* 2011, **32:** 459-474.

52.   Uotila P, Lynch AH, Cassano JJ, Cullather RI. Changes in Antarctic net precipitation in the 21st Century based on Intergovernmental Panel on Climate Change (IPCC) model scenarios. *Journal of Geophysical Research* 2007, **112:** D10107.

53.   Golledge NR, Marsh OJ, Rack W, Braaten D, Jones RS. Basal conditions on two Transantarctic Mountain outlet glaciers from observation-constrained diagnostic modelling. *Journal of Glaciology* in press.

54.   Golledge NR, Levy RH. Geometry and dynamics of an East Antarctic Ice Sheet outlet glacier, under past and present climates. *J Geophys Res* 2011, **116**(F3)**:** F03025.

55.   Cuffey KM, Paterson WSB. *The Physics of Glaciers, 4th edition*. Academic Press, 2010.

56.   Golledge N, Hubbard A, Bradwell T. Influence of seasonality on glacier mass balance, and implications for palaeoclimate reconstructions. *Climate Dynamics* 2010, **35**(5)**:** 757-770.

57.   Holland PR, Jenkins A, Holland DM. The response of ice shelf basal melting to variations in ocean temperature. *Journal of Climate* 2008, **21**(11)**:** 2558-2572.

58.   Oerlemans J. A flowline model for Nigardsbreen, Norway: projection of future glacier length based on dynamic calibration with the historic record. *Journal of Glaciology* 1997, **24:** 382-389.

59.   Oerlemans J, Anderson B, Hubbard A, Huybrechts P, Johannesson T, Knap W*, et al.* Modelling the response of glaciers to climate warming. *Climate Dynamics* 1998, **14**(4)**:** 267-274.

60.   Enderlin EM, Howat IM, Vieli A. The sensitivity of flowline models of tidewater glaciers to parameter uncertainty. *The Cryosphere* 2013, **7**(5)**:** 1579-1590.

61.   Anderson B, Lawson W, Owens I. Response of Franz Josef Glacier Ka Roimata o Hine Hukatere to climate change. *Global and Planetary Change* 2008, **63**(1)**:** 23-30.

62.   Oerlemans J. Climate sensitivity of Franz Josef Glacier, New Zealand, as revealed by numerical modeling. *Arctic and Alpine Research* 1997, **29**(2)**:** 233-239.

63.   Raper SCB, Braithwaite RJ. Glacier volume response time and its links to climate and topography based on a conceptual model of glacier hypsometry. *The Cryosphere* 2009, **3**(2)**:** 183-194.

64.   Fujita K. Effect of precipitation seasonality on climatic sensitivity of glacier mass balance. *Earth and Planetary Science Letters* 2008, **276**(1–2)**:** 14-19.

65.   Fujita K. Influence of precipitation seasonality on glacier mass balance and its sensitivity to climate change. *Annals of Glaciology* 2008, **48**(1)**:** 88-92.

66.   Huybrechts P. Sea-level changes at the LGM from ice-dynamic reconstructions of the Greenland and Antarctic ice sheets during the glacial cycles. *Quaternary Science Reviews* 2002, **21**(1-3)**:** 203-231.